Journal of Hydrology 631 (2024) 130798

Contents lists available at ScienceDirect

Journal of Hydrology

journal homepage: www.elsevier.com/locate/jhydrol

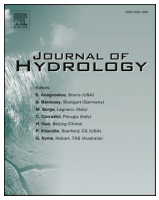

Measurement and analysis of the drag coefficient of wood accumulations at an ogee crested spillway

E. Persi *, E. Pibia, G. Petaccia, P. Ghilardi, S. Sibilla

Department of Civil Engineering and Architecture, University of Pavia, via Ferrata 3, Pavia, Italy

ARTICLE INFO

This manuscript was handled by Jesús Mateo-Lázaro, Editor-in-Chief, with the assistance of S. Sally Elizabeth Thompson, Associate Editor

Keywords:
Wood accumulation
Drag coefficient
Ogee crested spillway
Wood continuity

ABSTRACT

Trunks, branches, and wooden pieces transported by rivers during flood events can reach dams and accumulate at spillways. The reduced flow velocity and the presence of sluice gates may increase the probability of wood accumulation and gate malfunctioning. To prevent these effects, rakes or floating booms are installed upstream of the crest, thus requiring the removal of the accumulated material, and interrupting floating sediment continuity. An experimental campaign is carried out to increase the knowledge of the hydrodynamic behavior of wood jams upstream of an ogee-crested spillway. The drag coefficient for samples with different dimensions, roughness, submergence, and distance from the crest is measured under a hydraulic condition just below the one that, according to literature suggestions, should facilitate wood passage. The number of identical trials required to obtain statistically sound results is also analyzed. Experimental results show that the drag coefficient of wooden samples upstream of a spillway increases with the submergence of the samples and with the proximity to the spillway. The drag coefficient increases with submergence more than measurements in open-flow conditions, due to flow-wood-spillway dynamics. The distance from the spillway strongly affects the drag coefficient, followed by the shape and surface roughness. The blockage ratio for a spillway is defined, and the relation between the drag coefficient, the blockage ratio, and the non-dimensional distance is derived to compute the hydrodynamic force on a wood accumulation upstream of an ogee crested spillway.

1. Introduction

Wood in rivers positively affects the riverbed morphology and the flow patterns, playing an important role in long-term river dynamics due to the influence on erosion and sedimentation (Bocchiola et al., 2008, Spreitzer et al., 2021). When wooden material decomposes it also releases nutrients (Bocchiola et al., 2006), contributing to the nutrient balance of freshwater and aquatic life. In the past, large portions of wooden elements were removed from rivers to diminish wood-related hazard and improve navigability. To reduce the ecological impact of these management choices, many studies focused on the reintroduction of wood in rivers (Gippel et al., 1996), confirming the positive effects of wood on the freshwater ecosystem (e.g., Everall et al., 2012, Flores et al., 2011). Natural engineering practices employ wooden elements to restore river naturalness, while simultaneously reducing flood risk, with combined hydraulic and ecological benefits (e.g., Deane et al., 2021, Grabowski et al., 2019, Wenzel et al., 2014). Such practices agree with the definition of a "target wood regime", which aims at balancing benefits and potential hazards of wood, the latter being mainly connected to wood transport (Wohl et al., 2019).

In fact, during flood events, wooden pieces can be entrained from floodplain areas due to bank erosion and other gravitational phenomena. Entrained wood can be transported to bridge piers or dams, affecting the infrastructure safety and proper functioning (Bradley et al., 2005; Swiss Committee on Dams, 2017). Such issues can be further exacerbated by climate change, which modifies rainfall patterns and may give rise to intense or long-lasting precipitations, connected to extreme flooding (Dankers and Feyen, 2008). This may result in higher slope erosion and, consequently, large wood transport.

When the logs reach an infrastructure, the accumulation of a key element with additional medium and small wood pieces, leaves, and soil particles eroded from the bottom (Manners and Doyle, 2008), may trigger the formation of a log jam. Near urban areas, plastics and other anthropogenic debris may accumulate, too. The interaction between wood jam and infrastructures, including bridges, weirs and also buildings in the flooded areas (Korswagen et al., 2022), can cause local scour of bridge piers, overtopping, upstream flooding, or, in the worst-case scenario, the collapse of the infrastructure.

* Corresponding author.
E-mail address: elisabetta.persi@unipv.it (E. Persi).

https://doi.org/10.1016/j.jhydrol.2024.130798
Received 23 August 2023; Received in revised form 25 November 2023; Accepted 8 January 2024
Available online 29 January 2024

In fact, a large jam can reach a very low porosity and create an impermeable wall (Manners et al., 2007), forcing the water flow downward, eroding the bottom, especially at bridge piers, or leading to an increase in the water level upstream, both for a bridge or a dam, and consequently endangering the safety of neighboring human settlements. Disaster events in the past include, for example, the case of Palagnedra dam (1978, Switzerland), where overturning of the dam was at risk (Bruschin et al., 1982), and the case of Sa Teula dam (2005, Italy), in which the dam overloading led to the breaking of some gates (Wark et al., 2018). After the Vaia storm (2018, Italy, Chirici et al., 2019), large wood accumulation was observed at the Comelico dam, affecting the structures and the hydropower production. Similar events motivated the study of the interaction between debris and dam infrastructures aimed at quantifying the increase in the water level upstream of the spillway caused by a significant volume of wooden material. For example, Hartlieb (2017), Furlan et al. (2019), and Bénet et al. (2021) studied the backwater effect caused by the accumulation of wooden material at spillway's gates, under different hydraulic conditions (varying the Froude number, gate opening and number of wooden samples). The backwater effect appears to depend on the development and shape of the accumulation, and it increases with the Froude number (Hartlieb, 2017). Furthermore, Furlan et al. (2018) found that the backwater effect is linked to the probability of blockage which depends on the log size, being inversely proportional to the ratio between the water head on the spillway crest and the log diameter. The backwater effect is associated with a loss in the spillway flow rate, which may pose severe issues to the hydrodynamic response of the structure in case of extreme events. Bénet et al. (2021) evaluated the probability of blockage as a function of the gate opening and of the water head on the spillway, obtaining that the probability of blocking increases with the closing of the gates and the decrease of the water level on the spillway. Furthermore, they highlighted a reduction of about 23 % of the discharge coefficient if no countermeasures are adopted at the dam, possibly endangering the flow-peak reduction capacity of the reservoir.

The additional backwater effect induced at dams by the presence of wood accumulations may also influence the upstream reach. Liro et al. (2020) showed that backwater inundations due to a dam affect the hydrodynamics and morphology of the reservoir tributary, increasing channel-floodplain connectivity and sediment deposition. Such effects may be exacerbated if wood accumulations are present at the dam.

Regarding the interaction with infrastructures, the intensity of the hydrodynamic force exerted on the wood by the flow, which causes additional loads and backwater effects, depends on the flow conditions, the wood submergence, orientation, and the characteristics of the logs. Godtland and Tesaker (1994) propose an equation to account for the force of the water on a trash tangle, useful to dimension an anchoring system upstream to the structure. However, such equation does not consider the force that may arise when wood is near to the spillway.

To guarantee the safe passage of the trunks it is necessary to ensure the correct opening of the gates and an appropriate height of water on the spillway's crest, as stated by Godtland and Tesaker (1994) and Bénet et al. (2021). Suggested dimensions are generally based on experimental values and not linked to the analysis of the hydrodynamic forces that occur during the phenomenon. Nonetheless, such values are used as a benchmark in the design or operation of maintenance of dams in some European countries such as Switzerland and Austria (Swiss Committee on Dams, 2017). Clearly, the effectiveness of such procedure is essential for the structure safety as well as to reduce the impacts of dams on the wood regime.

The dynamics of wood accumulation at a spillway is still poorly investigated, especially concerning the hydrodynamic effects on wood accumulation and the forces potentially exerted on a structure. To contribute to this knowledge, the aim of this study is to investigate the interactions between wood and an ogee-crested spillway, to understand the variation of the hydrodynamic coefficients for different shapes and configurations of wood accumulations. This can provide useful insight for the design of dam protection strategies and for the procedures that ensure wood continuity. Moreover, the hydrodynamic coefficients are required to calculate the additional load on the structure and can be used in hydrodynamic modeling to estimate the backwater effect at the spillway. They can help define the conditions to ensure wood passage and reduce jeopardizing and endangering the proper spillway functioning.

2. Materials and methods

A series of experiments is performed to analyze the effect of the variation of several parameters on the hydrodynamic coefficients of wood accumulation upstream of an ogee crested spillway. The ogee crested spillway is selected because it is one of the most used structures for dam overflow as, being derived in its shape from the aerated nappe over a sharp-crested weir, it results in an almost atmospheric pressure over the crest for a specific design head (Badanapuri, 2019). The tests are performed with an undisturbed water elevation that corresponds to the design head and to low flow conditions that should ensure log accumulation (Bénet et al., 2021). The transversal dimension of the accumulation is based on the geometrical scaling used to design the spillway, to provide a reasonable dimension. The shape was varied from cylindrical to regular accumulation (based on Hartlieb, 2017), to a sort of regular accumulation of natural wood.

2.1. Experimental setup

The experiments are carried out in a laboratory flume of the Hydraulics Laboratory at the University of Pavia, 9.40 m long, 0.48 m wide (W) and with a maximum depth of 0.80 m (Fig. 1). The flume bottom is horizontal and metallic, and the side walls are made of polymethylmethacrylate (PMMA).

The flow rate is measured through a V-notch weir (Petaccia and Fenocchi, 2015), with the water head measured by a glass piezometer positioned laterally to the head tank (with a vernier scale, precision of ± 0.0001 m).

An ogee crested spillway model is placed about 6.5 m downstream of the weir. It was designed according to the guidelines developed by the U. S. Army Corps of Engineers (U.S. Army Corps of Engineers, 1990), with a vertical upstream wall and a curved profile given by:

$$X^{1.85} = 2H_d^{0.85}Y \tag{1}$$

where X and Y are the coordinates of the crest profile originating at the apex C of the crest, and H_d is the design head. Fig. 2 shows a picture of the spillway and the scheme of its theoretical cross section.

Considering the geometrical scales reported by Bénet et al. (2021), the model of the spillway has a distorted scaling: $\lambda_t = 109$ in the transversal direction; $\lambda_z = \lambda_l = 85$ in the vertical and longitudinal directions. It is 0.173 m high and 0.48 m wide, like the full flume width, and represents a prototype of a spillway with a length of 50 m and a height of 14 m. The scaling is not meant to represent an existing structure but rather aims to provide a comparison to a hypothetical prototype. The profile is obtained by adopting a design head of $H_d = 0.015$ m, a value close to the smallest undisturbed values used by Bénet et al. (2021) to test the blocking probability at a weir without piers. The spillway is anchored to a metal base to prevent tipping and sealed to the channel walls. The skeleton of the structure is formed by wooden supports and is covered with PMMA to replicate a hydraulically smooth model.

The hydraulic conditions are set to have $H_W/H_d = 1$, where H_W is the water head upstream of the weir minus the weir elevation. The length of the samples is 0.15 m in the model, which corresponds to 16 m in a prototype according to the transversal geometrical scaling, comparable to the maximum length of the logs observed in wood accumulations at weirs in Switzerland, i.e., 11 m by Bezzola and Hegg (2007) and 15 m by

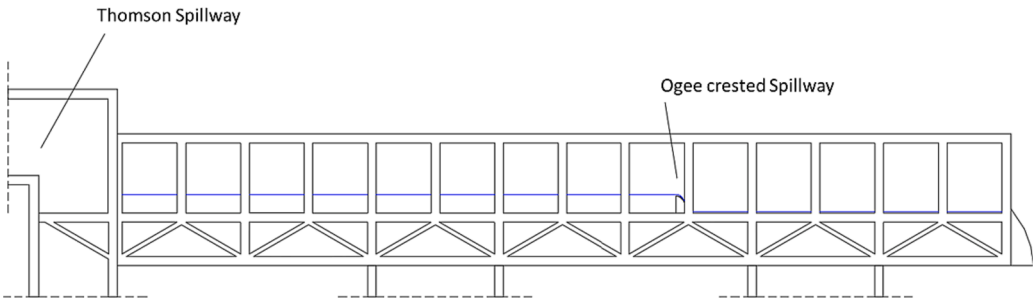

Fig. 1. Simplified longitudinal section of the laboratory flume.

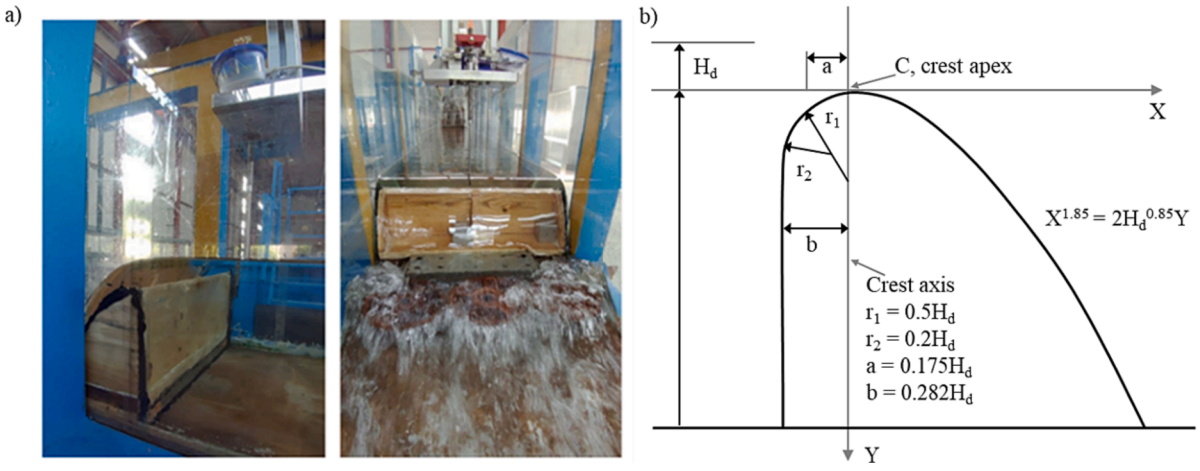

Fig. 2. A) ogee crested spillway installed into the laboratory channel (lateral and frontal view); b) wes ogee crested profile with the vertical upstream wall (). adapted from Badanapuri, 2019

Rickli and Hess (2009). The vertical dimension cannot be compared as information about the height of real log accumulation at spillways is not provided. Considering the distorted scale, the ratio between the design head and the log length in a prototype is $H_{d,p}/L_p = 7.8$ %, slightly lower than the ratio that should be guaranteed to ensure the safe passage of logs downstream of a spillway without a superstructure ($H = 10$ % of L, Godtland and Tesaker, 1994; Hartung and Knauss, 1976). Based on the spillway design head and on the log length, the model replicates the possible conditions of wood accumulation at a weir without superstructures.

To measure the force exerted by the flow a hydrodynamic balance, designed at the Hydraulics Laboratory of the University of Pavia (Fig. 2a), is installed just upstream of the weir, with a distance variable depending on the sample's dimension. It is based on a leverage system with 4 load cells that measures the horizontal components of the hydrodynamic force, namely the drag and side force, which vary according

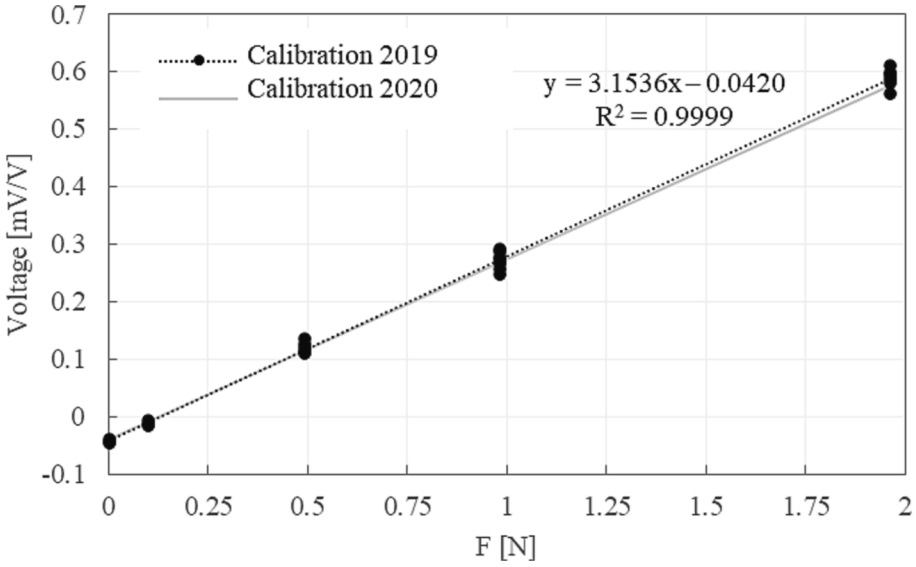

Fig. 3. Calibration curves for the cell that measures the drag force.

to the sample orientation and submergence. The instrument has an operational range of 0.03–2 N and a relative uncertainty of about 8.1 % and 11.7 % for the drag and side coefficients, respectively. In this campaign, only the drag component is measured, as the samples are symmetrical to the flow, so that the transversal forces are balanced. Further details about the functioning of the balance are provided by Persi et al. (2019). In the experimental campaign the logs are near the spillway, the wood accumulation orientation is kept constant, perpendicular to the flow, and only the drag force is measured. The instrument measures a differential voltage that is converted into the drag force thanks to the calibration curve shown in Fig. 3. The present calibration curve is displayed together with a previous one (2019) since periodic repetitions of the calibration procedures are performed to check the system conditions.

The drag coefficient C_D is obtained from the measured drag force F_2 as:

$$C_D = \frac{F_2}{\frac{1}{2}\rho A_{log} V_S^2} \tag{2}$$

where ρ is the density of the fluid, the area $A_{log} = LD$ represents the cross-section of the sample, and $V_S = Q/(WH_W)$ is the theoretical flow velocity on the spillway, given by the continuity equation. The product between the effective width of the spillway, which coincides with the channel width, W, and H_W, that represents the water total energy upstream of the spillway minus the weir elevation, is the undisturbed cross-section above the crest. The velocity V_S is the theoretical maximum speed on the crest, which is the simplest velocity to calculate, the most stable, and the most significant to describe the interaction between the logs and the spillway. Upstream of the spillway the velocity is lower (the bulk velocity in the channel is about 0.019 m s^{-1}), and the velocity fields are complex, developing in the three spatial directions so that the quantification of a reference velocity in the longitudinal direction would be unreliable and of little practical importance. The reference area for drag computation is the longitudinal section of the sample, even if the sample is not fully submerged. This encloses all the uncertainties related to body shape, roughness, and also submergence within the drag coefficient and eases the comparison with the coefficients for submerged cylinders.

The drag coefficient is evaluated for single wood accumulations, varying the size, and the surface and shape roughness. First, cylindrical samples are employed as a reference. These samples are not meant to represent single logs (that would be unrealistic at prototype scale), rather they represent the non-porous frontal obstruction of a wood accumulation. Their simplified geometry helps in focusing on the obstruction-spillway interaction dynamics, and on the effect of the vertical size. Then, the effect of surface roughness and shape roughness is analysed using a rough cylinder and log jams with comparable dimensions and volumes. All the samples have the same length, $L = 0.15$ m.

As shown in Fig. 4, two smooth cylindrical samples and a rough one are used:

- *Smooth small* log: $D = 0.023$ m (Fig. 4a-b).
- *Smooth medium* log: $D = 0.042$ m (Fig. 4c-d).
- *Natural medium* log: $D = 0.037$ m, (Fig. 4e-f).

According to the geometrical scaling ratios, the samples represent prototype obstructions with a transversal span of about 16 m and a vertical size in the range 1.9–3.6 m, higher than the 1.27 m free water span above of the spillway (which is the value equivalent to $H_W = H_d = 0.015$ m in the model). Such obstructions represent wood accumulations with a significant vertical dimension as those that may be originated from wood with heavier density (Hartlieb, 2017).

Pre-formed wood jams were used to measure the hydrodynamics coefficients of accumulations. Cylinders with a length of 0.15 m were glued to create a solid wood jam with a triangle-like cross section, as shown in Fig. 5, either with smooth cylinders (Fig. 5a-c, *Smooth wood jam*, average diameter $D_{avg} = 0.005$ m) or natural ones (Fig. 5d-f, *Natural wood jam*, $D_{avg} = 0.006$ m). According to the distorted scaling ratios adopted for the model, they correspond to a log prototype about 16 m long and with diameter of about 0.45 m. The triangular cross-section of the wood jams was adopted according to the studies of Panici and de Almeida (2018), in which the dynamics of the formation of log jams at bridge piers are studied and a methodology for determining their dimensions is provided. To maintain similar dimensions to those of the single logs described above, the log jams are characterized by the ensemble dimensions shown in Table 1, where H_{jam} is the maximum vertical height, K_{jam} is the maximum longitudinal extension, and L_{jam} is the transversal dimension, equal to the length of the log.

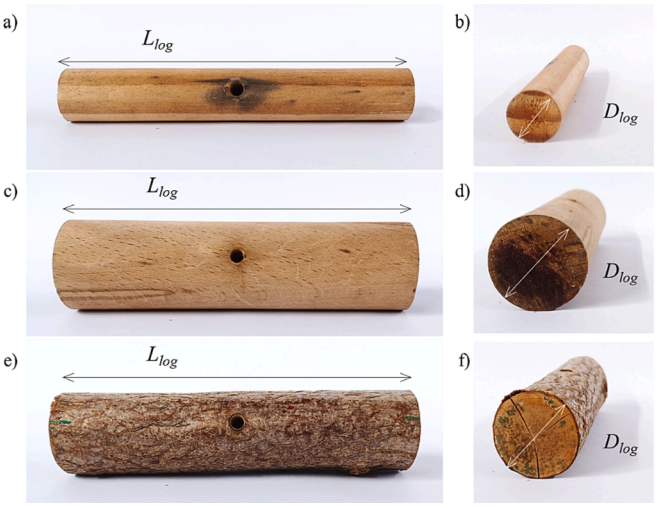

Fig. 4. Top-view and cross-section of the (a, b) Smooth small log; (c, d) Smooth medium log and (e, f) Natural medium log.

2.2. Minimum number of repetitions

A statistical analysis was carried out to assess the minimum number of tests required to obtain a statistically valid average value, i.e., independent of the size of the sample (number of acquired data), mediating operator, or instrumental inaccuracies of the individual experiments. To this aim, a series of 150 repetitions was acquired by placing the *Smooth medium* log fully submerged at a distance of 0.01 m upstream of the spillway. The drag force was measured with a time interval of 30 s, and the drag coefficient was computed for each repetition from the time-averaged value. The balance was unloaded by dethatching the pressor from the cells after each repetition, to avoid any creeping effect.

Through the statistical computation of the upper and lower limits of the drag coefficient distribution (25 % quartile minus 1.5 times the interquartile range, and 75 % quartile plus 1.5 times the interquartile range), 9 outliers above 1.601 were excluded from the distribution to avoid biasing the overall average. With the new sample of 141 measurements, the average value for a progressively growing number of experiments (from 10 to 141) was computed and compared to the overall average by calculating the percentage absolute error, according to the equation:

$$error(n) = \frac{\left(C_{D,avg.n} - C_{D,tot}\right)}{C_{D,tot}},\ n = 10 - 141 \tag{3}$$

where n is the number of repetitions, $C_{D,avg.n}$ is the average drag coefficient computed for n repetitions and $C_{D,tot}$ is the overall average. Fig. 6a shows the measured drag coefficients with the overall average, while Fig. 6b and 6c show the trend of the average and of the error when

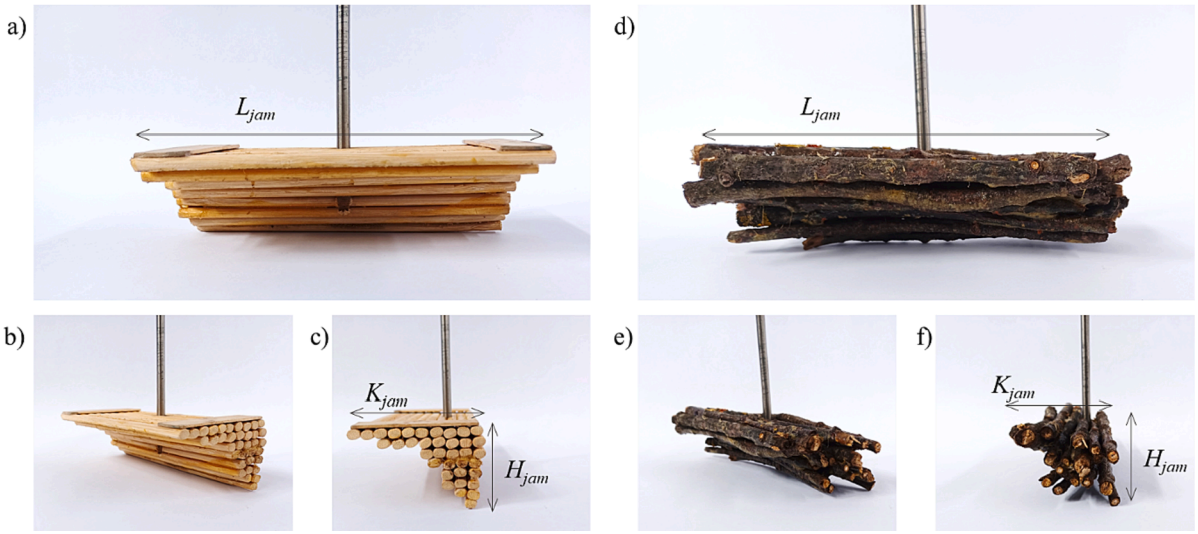

Fig. 5. A) frontal, b) oblique and c) cross-sectional view of the *Smooth wood jam*; d) frontal, e) oblique and f) cross-sectional view of the *Natural wood jam*.

Table 1
Log jams dimensions.

Sample	H_{jam} [m]	K_{jam} [m]	L_{jam} [m]
Smooth wood jam	0.039	0.065	0.15
Natural wood jam	0.035	0.050	0.15

increasing the number of the experiments. The error becomes lower than 1 % for more than 56 experiments, thus 60 repetitions were carried out for each configuration in the current experimental campaign.

2.3. Experimental campaign description

The tests were carried out under steady-state conditions, with a flow rate range of 1.5–1.8 L/s, measured with a glass piezometer upstream of the V-notch weir, and an average water level $h = 0.189$ m in the approach channel, measured with a graduated rod (±0.0005 m). The bulk velocity in the approach channel is about 0.019 m s^{-1}, so the water energy coincides with the water level, and the value above the crest, H_W, corresponds to the design head $H_d = 0.015$ m ($H_W/H_d = 1$). The velocity on the crest is $V_s = 0.21$–0.25 m/s and the Froude number on the crest is $Fr = V_s/\sqrt{gH_W} \cong$ 0.54–0.63. The computed discharge coefficient, C_{dis}, derived from the equation:

$$Q = \frac{2}{3} C_{dis} B \sqrt{2g} H^{1.5} \tag{4}$$

is in the range 0.59–0.69, lower than the expected value of 0.74 for an ogee weir at head conditions (SI units, U.S. Bureau of Reclamation,

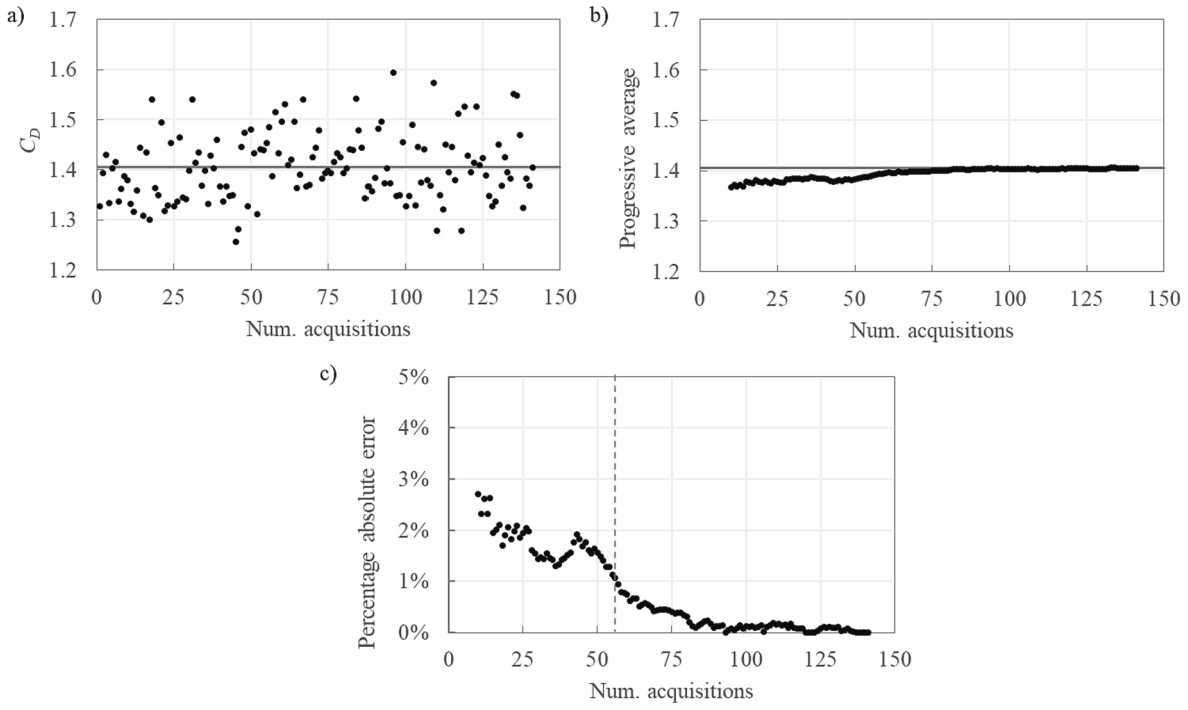

Fig. 6. A) drag coefficient (black dots) and overall average value (grey line) excluding the outliers; b) progressive average (black dots) versus overall average (grey line); c) percentage absolute error of the progressive average with respect to the overall average. the red dashed line shows when the error becomes smaller than 1%.

1987, Vischer and Hager, 1998, Salmasi and Abraham, 2020). Flow rate and water level variations between the tests were observed, as the flume was set near its lowest limit of stable flow rate. The actual hydraulic parameters for the computation of the flow velocity were updated for each repetition, to ensure the most accurate estimate of the drag coefficient.

The measurement of the drag coefficient was performed by placing the wooden samples either at different submergence values (Set 1) or at different distances from the spillway (Set 2). In Set 1, by maintaining a constant distance of 0.01 m between the downstream edge of the samples and the spillway crest, three submergences were tested, i.e., $\sigma = \frac{D_{wet}}{D_{log}} = 1, 0.75, 0.5$ (D_{wet} being the submerged part of the log diameter) as shown in Fig. 7a-b-c. The sample elevation was set considering the undisturbed water level.

Set 2 was carried out by fixing the submergence of the samples ($\sigma = 1$, fully submerged) and varying the distance Δ between the samples and the spillway (Fig. 7d). A maximum distance of about 0.03 m was tested, because at higher distances the hydrodynamic force is small due to the small water velocity, reaching the instrument detection limit. Note that the different dimensional distances Δ were selected to maintain fixed values of the non-dimensional distance $\eta = \frac{\Delta}{D_{log}}$, except for the smallest value that ranges between 0.10 and 0.17 based on the sample diameter, corresponding to a minimum distance of about 4–5 mm.

The drag force was measured for both cylindrical samples and wood jams. For the latter, the samples were positioned by placing the upper cylinders semi-submerged, while the rest of the jam remained below the water surface.

Table 2 shows the tested configurations for both experimental campaigns. The log Reynolds number computed with the crest velocity (either $Re_p = \frac{V_s D_{log}}{\nu}$ for cylinders or $Re_p = \frac{V_s H_{jam}}{\nu}$ for wood jams) is also shown. By combining the different samples and test configurations, 30 different tests were performed. For each test, the average drag coefficient was obtained as the average of about 60 repetitions, that were performed in different sessions by alternating the samples, to avoid errors due to creeping and considering possible slight variations of the configuration.

3. Results and discussion

3.1. Drag coefficient variation with submergence and proximity

The average drag coefficient C_D and the standard deviation for Set 1 are shown in Table 3 as a function of submergence. Overall, the drag coefficient increases with submergence for all the samples, and the standard deviation is generally higher for increasing submergence, except for the *Smooth medium* log that presents a higher standard deviation for $\sigma = 0.75$.

Considering the variation of the drag coefficient as a function of the sample type, the trend is not fully clear. The smooth samples should present similar results, as the diameter variation is already taken into consideration in Eq. 2. Observing our results, this is true for $\sigma = 1$, while for other submergence values some differences are observed. For the half-submerged configuration, this relates to the very small forces detected with the *Small smooth* log, which are close to 0.03 N, that corresponds to the instrument zero balance. For this reason, such a value is considered poorly accurate and is shown in italics in Table 3. For $\sigma = 0.75$ the measured values are in a small range, with comparable standard deviation, and a clear differentiation between the behaviour of each sample is not possible.

Considering the medium logs, the effect of surface roughness, higher for the natural sample, appears to be significant only for the fully submerged configuration. The *Natural medium* log presents the highest measured value but shows also the highest standard deviation among the tests of Set 1.

Table 4 shows the average drag coefficient and the variance resulting from Set 2. The drag coefficient decreases with the distance from the spillway, due to the decrease of the flow velocity upstream of it. In fact, the crest velocity used to calculate the drag coefficient (Eq. 2) is kept almost constant in the range 0.21–0.25 m/s for the different trials, while the bulk velocity in the channel upstream of the spillway is much smaller, around 0.019 m/s. Thus, a significant velocity reduction occurs when the distance from the spillway increases, that reflects on a smaller hydrodynamic force and a smaller drag coefficient.

Also in this case, the surface roughness contributes to increasing the drag coefficient, with the *Natural medium* log presenting higher values than the *Smooth medium* log. However, the distance plays the major role in drag variation.

Regarding the wood jams, the drag coefficients of the *Smooth wood jam* are near those of the *Natural medium* log, while the *Natural wood jam* presents the lowest values for each distance, probably because of the spacing between the single elements composing the jam. Due to this

Table 2
Summary of the experimental setup.

Sample	Set 1 σ ($\Delta = 0.01$ m)	Set 2 η ($\sigma = 1$)	Re_p [-]
Smooth small log	1, 0.75, 0.5	0.17, 0.25, 0.40, 0.55	5.5×10^3
Smooth medium log	1, 0.75, 0.5	0.10, 0.25, 0.40, 0.55, 0.7	1.0×10^4
Natural medium log	1, 0.75, 0.5	0.14, 0.25, 0.40, 0.55	8.9×10^3
Smooth wood jam	–	0.10, 0.25, 0.40, 0.55, 0.7	9.4×10^3
Natural wood jam	–	0.25, 0.40, 0.55	8.4×10^3

Table 3
Average drag coefficient and standard deviation in brackets for the experiments of Set 1. In italics, poorly accurate data.

Sample	σ [-]		
	0.5	0.75	1
Smooth small log	*0.26 (0.071)*	1.04 (0.095)	1.57 (0.093)
Smooth medium log	0.40 (0.023)	1.20 (0.077)	1.55 (0.043)
Natural medium log	0.41 (0.045)	1.12 (0.062)	1.81 (0.149)

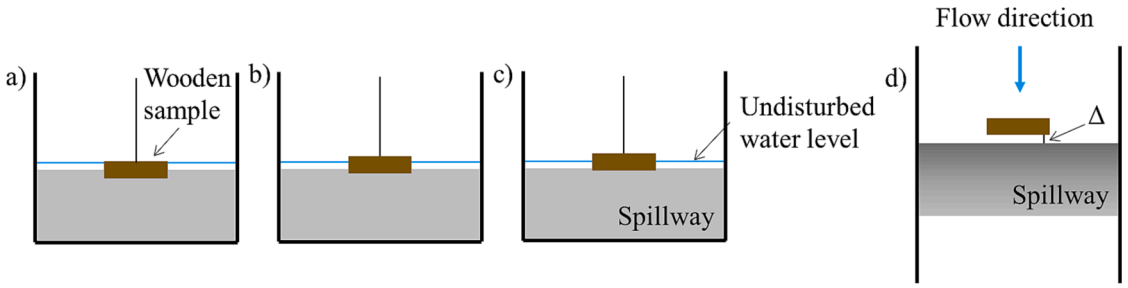

Fig. 7. Scheme of the experimental configuration with the smooth large sample ($D_{log} = 0.042$ m): cross section for a submergence: a) $\sigma = 1$, b) $\sigma = 0.75$, c) $\sigma = 0.50$; d) top-view showing the distance between the sample and the crest of the spillway, set equal to 0.01 m for the Set 1, and variable in Set 2.

Table 4
Experimental results for Set 2.

Sample	η [-]	Δ [m]	C_D [-]	σ_D [-]
Smooth small log	0.17	0.004	3.45	0.390
	0.25	0.006	2.81	0.235
	0.40	0.009	2.03	0.273
	0.55	0.013	1.32	0.223
Smooth medium log	0.10	0.004	3.12	0.350
	0.25	0.010	1.41	0.106
	0.40	0.017	0.81	0.100
	0.55	0.023	0.47	0.062
	0.70	0.029	0.27	0.018
Natural medium log	0.14	0.005	3.33	0.190
	0.25	0.009	1.97	0.226
	0.40	0.015	1.36	0.174
	0.55	0.020	0.79	0.194
Smooth wood jam	0.10	0.004	4.30	0.233
	0.25	0.010	2.20	0.259
	0.40	0.015	1.34	0.159
	0.55	0.021	0.79	0.091
	0.70	0.027	0.44	0.082
Natural wood jam	0.25	0.009	2.28	0.307
	0.40	0.014	1.08	0.102
	0.55	0.019	0.67	0.049

higher porosity, the hydrodynamic resistance of the sample is lower, especially when increasing the distance from the spillway (Table 5).

3.2. Comparison with literature data and generalization

The increase of the drag coefficient with the sample submergence agrees with literature findings for isolated cylinders in uniform open-channel flow conditions. Ren et al. (2019) obtained drag coefficients of 1.2, 0.7 and 0.31 for a smooth cylinder with submergence of 1.0, 0.75 and 0.50, respectively, and a particle Reynolds number in the range 4.4 x 10^4 – 8.8 x 10^4. Persi et al. (2019) also obtained drag coefficients increasing with submergence (1.21 and 0.6 for 1.0 and 0.5 submergence, respectively), for a log with D_{log} = 0.024 m and a particle Reynolds number of 1.0 x 10^4. The increasing trend of the C_D with increasing submergence is justified by the larger area exposed to the flow, that results in a stronger deflection of the fluid lines, energy loss and pressure unbalance between the upstream and downstream sides of the sample. This is also related to the use of the sample cross-section shown in Eq.3. The rate of increase of the drag coefficient with submergence remains below 2 (1.2 and 1.7 for Persi et al. (2019) and Ren et al. (2019), respectively) for uniform open-channel flow conditions, while for the present results in the flow over a spillway, it ranges between 2.1 and 2.8, as shown in Fig. 8.

This may be connected to the interaction between the log and the spillway. The pressure distribution on the ogee crested spillway depends on the hydraulic head, with nearly zero relative pressure if the head corresponds to the design head, and even negative relative pressures for higher heads, as those that may be induced by the presence of an obstacle that partially occludes the flow passage. In addition, when the submergence increases, the sample further deviates the flow and reduces the free area between the spillway and the sample itself, inducing further acceleration and reduction in static pressure.

The larger difference in pressure distribution due to the

Table 5
Parameters of the exponential curves in Fig. 9.

Samples	D_{log}[m]	a[-]	b[-]	R^2[-]
Smooth small log	0.023	5.284	−2.480	0.997
Smooth medium log	0.042	4.216	−3.996	0.988
Natural medium log	0.037	5.050	−3.370	0.981
Smooth wood jam	0.038	5.951	−3.716	0.995
Natural wood jam	0.035	6.115	−4.119	0.990

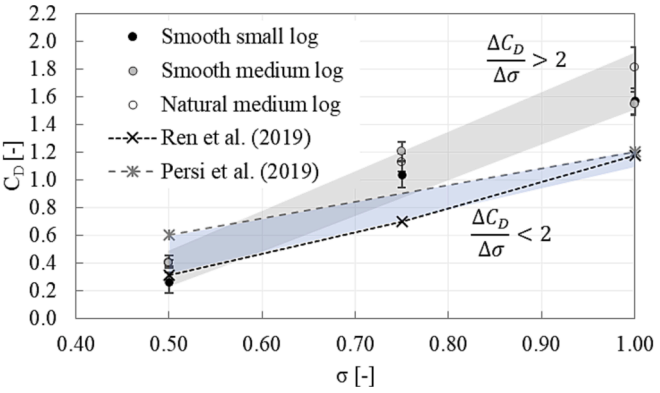

Fig. 8. C_D variation with submergence for the present study and literature data for cylinders in uniform open-channel flow conditions. Solid areas show the groups of data with a rate of increase lower and higher than 2.

aforementioned phenomena may be the reason of the steeper drag coefficient increase observed in Fig. 8. In an open-channel flow, flow diversion, free span variation, and surface waves, the main reasons for drag increase with submergence, are expected to be milder than in presence of a spillway.

Log accumulations near a spillway are expected to experience a higher drag force if they span vertically from the free surface to below the weir crest. Moreover, as shown by the experiments of Set 2, the drag coefficient increases for log accumulations approaching the spillway. Fig. 9 shows the measured drag coefficient as a function of the distance Δ (Fig. 9a) and of the dimensionless distance η (Fig. 9b). Both graphs show that, overall, the drag coefficient and the standard deviation decrease with distance. The smooth logs present the lowest values for every distance, while the *Natural medium* log and the *Smooth wood jam* present nearly overlapping coefficients, except for the smallest distance. This shows that the surface roughness and the shape roughness have a similar

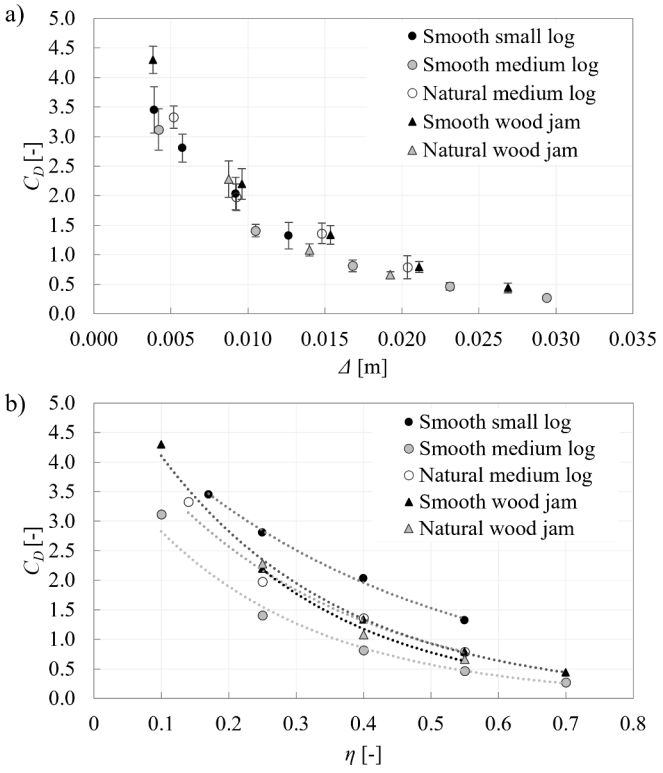

Fig. 9. C_D variation due to sample distances to the spillway: a) dimensional distance Δ; b) non-dimensional distance parameter η.

effect on the hydrodynamic resistance up to a certain distance from the spillway (about $\eta = 0.2$). Such a behaviour may justify the employment of natural circular samples to represent wood jams in experimental campaigns, to avoid issues related to the assembly of the samples and to the uncertainties of the proper shape to be assigned.

Lower values, comparable with those of smooth logs, are found for the *Natural wood jam*, which is a "rough" sample (due to both surface and shape roughness) but presents a higher porosity compared to the *Smooth wood jam* (see Fig. 5 for comparison). As anticipated, the porosity reduces the obstruction to the flow, therefore the drag force and coefficient remain lower. This agrees with the findings of Müller et al. (2022), who examined the effects of engineered log jams with different porosity, observing a higher hydrodynamic resistance, hence a higher backwater effect, for the non-porous structure with respect to the porous one.

Fig. 9b shows the same drag coefficients plotted against the dimensionless distance, which includes the effect of the diameter. Such representation highlights that for the *Natural medium* log and *Smooth wood jam*, which are slightly smaller than the medium smooth log, the C_D trend is overlapping and in an intermediate position with respect to the two smooth cylinders.

Exponential interpolation curves $C_D = ae^{b\eta}$ derived from Fig. 9b can be employed to estimate the expected drag coefficient for accumulations with other vertical dimensions or other dimensionless distances within the tested range. Fig. 10 shows the variation of the curve constants a and b with the ratio D_{log}/H_d or H_{jam}/H_d, a proxy of the vertical blockage of the flow area due to the samples. The constant a decreases with this ratio, and appears to be affected by the shape of the sample, presenting the highest value for the *Natural wood jam*. The exponent b decreases linearly with increasing ratio, except for the *Natural wood jam* that shows a value lower than expected. Due to these trends, the curves tend to be flatter and higher for little vertical obstructions, while their curvature increases for larger vertical size or irregular shape, resulting in a stronger variation of the coefficients as a function of the non-dimensional distance.

The application of the exponential curves to a prototype scale is straightforward if the Froude similarity is assumed, since both the drag coefficient (Wallerstein et al., 2001) and the non-dimensional distance are unchanged after scaling, as shown by Eqs. 5–6. Note that the fluid density and the gravitational acceleration are the same in model and prototype.

$$C_D = \frac{2F_D}{\rho LDV^2} = \frac{\lambda_f \lambda_z^2}{\lambda_f \lambda_z \lambda_z} = 1 \tag{5}$$

$$\eta = \frac{\Delta}{D} = \frac{\lambda_l}{\lambda_z} = \frac{\lambda_z}{\lambda_z} = 1 \tag{6}$$

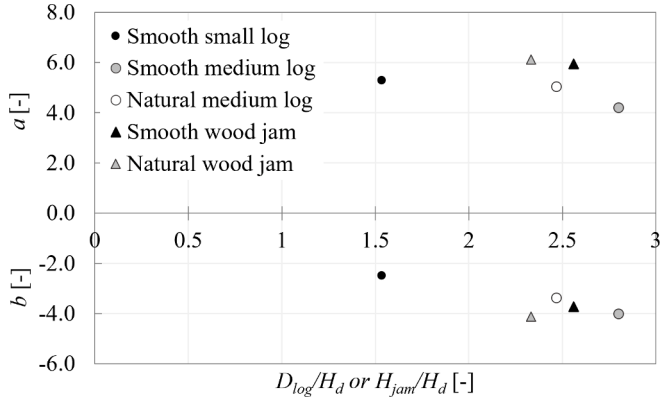

Fig. 10. Variation of the parameters a and b as a function of the ratio between the diameter, or height, of the sample and the design head.

For real wood jams, the adoption of the *Smooth* or the *Natural wood jam* parameters should be considered based on the expected amount of fine debris that may occlude the wood jam pores. However, an in-depth analysis of the effect of porosity on the hydrodynamic resistance, and yet on the parameters of the exponential curves, should be performed. In addition, limitations to the adoption of the Froude similarity and their consequences on model application to prototype scales are discussed in Paragraph 3.4.

3.3. Accounting for the blockage effect

The relation between the drag coefficient and the blockage effect due to the wood accumulation was developed by Gippel et al. (1996) for single and stacked cylinders without obstacles downstream, for a Froude number of 0.35 and blockage ratios in the range 0.03–0.3. The relation considers the drag coefficient C_D' in open-flow field conditions (cross-section sufficiently large not to affect the force on the sample, $C_D' = 1.2$) and the blockage ratio ($B = \frac{L_{log} D_{log}}{A}$, where A is the flow cross-section). The application of this equation helps in estimating the expected drag coefficient for different blockage ratios in open channels, but a similar relation for accumulations near a spillway is currently missing.

To fill this gap, first, the blockage ratio in the case of a spillway should be defined. As previously observed, the hydraulic conditions on the crest are the most stable for the flow over a spillway. In fact, upstream flow depends upon the basin geometry and may be more difficult to be generalized. For this reason, the flow area above the crest is here defined as the reference area for the computation of the blockage ratio for a spillway, that results:

$$B_{spillway} = \frac{LD}{BH_d} \tag{6}$$

where L and D represent the transversal and the vertical dimension of the accumulation, respectively. In the present experimental campaign, they coincide with the length and vertical size of the samples, as described in Paragraph 2.1, and the blockage at the spillway ranges between 0.48 and 0.88. Note that the area above the crest is constant, so that the blockage ratio variation is related to the change of the diameters or height of the samples. The blockage ratios are thus directly related to the samples, i.e., 0.48 for the *Smooth small* log, 0.77 for the *Natural medium* log, 0.8 for the *Smooth wood jam* and 0.875 for the *Smooth medium* log. The *Natural wood jam* is not considered in this analysis, due to the different hydrodynamic characteristics related to porosity.

In Fig. 11a the drag coefficients for single cylinders and for the *Smooth wood jam* (highlighted by a dashed line) are plotted against the blockage ratio, and according to the non-dimensional distance from the spillway (η).

The increase of the non-dimensional distance η brings to a decrease of the drag coefficient for the same blockage ratio. For the cylindrical samples, the difference between the maximum and the minimum drag coefficient, for the nearest and farthest position, respectively, is nearly constant, around 2.1–2.8 for the same blockage ratio. The results for the *Smooth wood jam*, highlighted with the blue dashed line in Fig. 11a, show a much sharper increase of the drag coefficient for decreasing non-dimensional distance, with a span of about 3.9 between the maximum and minimum coefficient. This is related to the shape of the accumulation, which tends to deviate downward the flow more strongly than the cylindrical samples, causing greater interaction between the sample and the spillway at the smaller distances.

For the same non-dimensional distance, a decrease of the drag coefficient for increasing blockage ratio is observed. This appear unexpected, as usually the increase of the blockage ratio is connected to an increase of the hydrodynamic coefficients (Gippel et al., 1996, Altinisik et al., 2015). In our study, however, the blockage increase is connected to an increase of the diameter and a consequent increase of the distance from the spillway (Δ), as the non-dimensional distance (η) is constant.

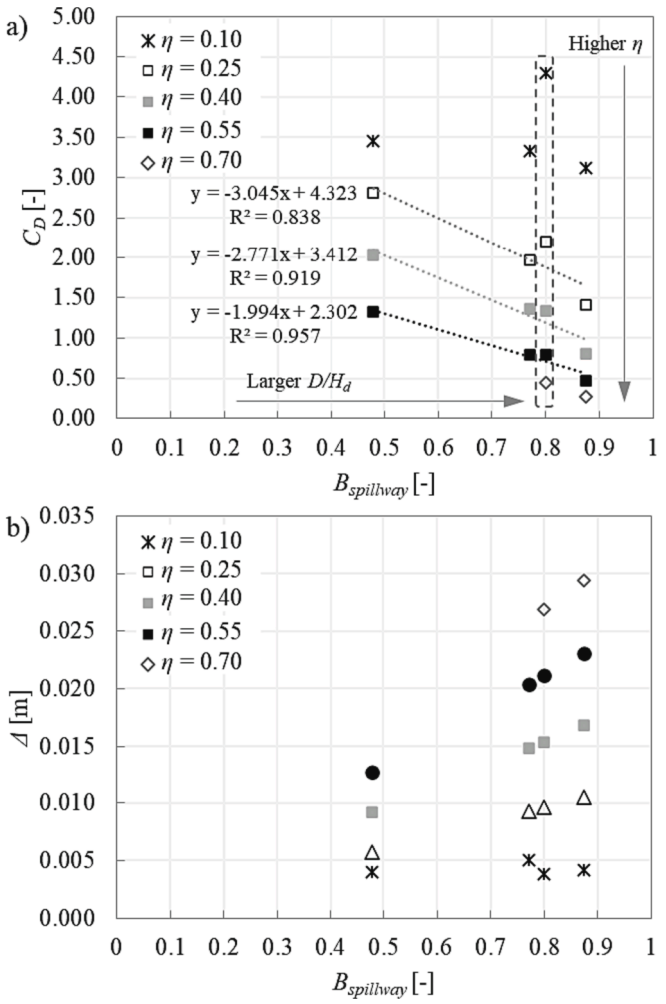

Fig. 11. A) drag coefficient as a function of the blockage ratio on the spillway and of the non-dimensional distance. the blue dashed line highlights the drag coefficients for the *Smooth wood jam*, and b) Dimensional distance as a function of the blockage and of the non-dimensional distance.

Fig. 11b shows that the dimensional distance increases with the blockage ratio, for the same non-dimensional distance. For the same η, a larger sample is farther away from the spillway and is subject to smaller flow velocity compared to a small sample size. This justifies the reduction of the drag coefficient for increasing blockage ratio and highlights that the proximity to the spillway is the most significant parameter for the variation of drag coefficient of an upstream accumulation.

Linear interpolations are provided for the most consistent data, i.e. for $\eta = 0.25$ to 0.55, and can be useful to define the drag coefficients for real accumulations, given the real dimensions of the spillway (design head and width), the wood accumulation (vertical height and transversal width) and the distance. Despite the geometrical scaling being distorted in the transversal direction, the nondimensional numbers η and B remain the same, as the shown by Eqs. 6 (in the previous paragraph) and 8:

$$B_{spillway} = \frac{LD}{BH_d} = \frac{\lambda_l \lambda_z}{\lambda_l \lambda_z} = 1 \tag{8}$$

This allows the direct extension of the relations shown in Fig. 11 at prototype scale.

3.4. Scale effects and application ranges

As the tests are performed at an ogee crested spillway without bays, relatively low flow is imposed to remain within the log accumulation conditions, as shown by Bénet et al. (2021). Such conditions lead to low Reynolds number ($Re = \frac{V_s h_s}{\nu}$, 3.13–3.75 × 10^3, where $h_s = 0.015$ m) and Weber number on the crest ($We = \frac{\rho V_s^2 h_s}{\sigma_f} = 11$, where ρ is the fluid density, $\sigma_f = 0.0722$ N/m is the surface tension,). The flow Reynolds number satisfies the critical value of 1400 suggested by Allen (1947) to avoid scale effects physical models in straight channels, but both the Reynolds and the Weber numbers are lower than the threshold values reported in Saneie et al. (2016): $Re < 10^5$ and $We < 500$ for morning glory spillways (Fais and Genovez, 2008) and and $Re < 10^5$ and $We < 100$ for two-phase stepped spillways (Boes and Hager, 2003). Saneie et al. (2016) showed that the scale effects are limited for values of $Re = 3.1 \times 10^4$ and $We = 270$, for an ogee weir with converging training walls. Erpicum et al. (2016) suggested a minimum Weber number (computed under critical conditions) of 54 for a key-piano weir, while Pfister and Schleiss (2013) suggested a flow depth of 0.015 m to avoid viscous effects for the same type of structure. Despite the conditions in the present model satisfy the limits proposed by Pfister and Schleiss (2013) and Allen (1947), the Reynolds and Weber numbers are lower than those generally reported to avoid scale effects.

As scale effects tend to increase the head (i.e., false head), thus affecting the weir rating curve, the hypothetical prototype's flow rate should not scale according to the Froude similarity. Considering a prototype at design conditions (with $H/H_d = 1$, as in our experiments) the flow rate without scale effect can be obtained by Eq. 4 with the standard discharge coefficient, $C_{dis} = 0.74$, with the weir dimensions scaled according to the geometrical factors. Table 6 shows the main parameters of the model, and of a prototype either scaled according to the Froude similarity (Prototype I), or taking into account only the geometrical ratios (Prototype II). In the latter, the Froude and Reynolds numbers are slightly higher, although in line with those obtained in Prototype I by applying the Froude similarity.

The particle Reynolds number range in our model is in line with Wallerstein et al. (2001) and Wallerstein et al. (2002), while the particle Froude numbers are slightly smaller, possibly leading to the underestimation of the drag coefficient. Wigley (1953), Khader (1979) and Wallerstein et al. (2002) agree that the drag coefficient, especially for samples near the water surface, shows a maximum around $Fr_p = 0.5$. Khader (1979) shows a drag coefficient increase of about 20 % from $Fr_p = 0.4$ to $Fr_p = 0.5$, for a submergence around 1.1 the sample diameter.

Table 6
Comparison among the main parameters of the model, of hypothetical prototypes scaled with the Froude similarity (Prototype I) and only geometrically (Prototype II).

Parameter	Symbol and units	Model	Prototype I	Prototype II
Spillway width	B_e [m]	0.48	52.32	52.32
Spillway crest height	P [m]	0.173	14.71	14.71
Design head	H_D [m]	0.015	1.275	1.275
Test head	H [m]	0.015	1.275	1.275
Flow rate	Q [m^3 s^{-1}]	0.0015–0.0018	128–153(*)	162
Flow velocity on the crest	V_s [m s^{-1}]	0.21–0.25	1.92–2.30(**)	2.43
Flow Froude number	Fr [-]	0.54–0.63	0.54–0.63	0.69
Flow Reynolds number	Re [-]	3.1–3.8 × E^3	2.4–2.9 × E^6	3.1 × E^6
Particle Froude number	Fr_p [-]	0.32–0.43	0.32–0.43	0.41–0.55
Particle Reynolds number	Re_p [-]	5.6 × E^3–1.0 × E^4	3.8–6.9 × E^6	4.8–8.9 × E^6
Sample's length	L [m]	0.15	16.35	16.35
Sample's height	D [m]	0.023–0.042	1.9–3.6	1.9–3.6

(*) flow rate ratio being $\lambda_z^{3/2}\lambda_l$,
(**) flow velocity ratio being $\lambda_z^{1/2}$.

Despite similar analysis are not available for half-submerged logs upstream of a spillway, it is likely that the values computed in the present experimental campaign underestimate the drag coefficients due to reduced particle Froude number.

Overall, in a prototype scaled with the Froude similarity (like Prototype I) the effect of viscosity is underestimated, and the flow velocity and particle Froude number are lower than in a prototype scaled only with geometrical ratios, and with a rating curve without viscous effects (like Prototype II). As the velocity is 25 % lower ($\Delta V = \frac{(V_{PrI}^2 - V_{PrII}^2)}{V_{PrII}^2}$, 2.11 m s^{-1} and 2.43 m s^{-1} in Prototypes I and II, respectively), the drag force should scale accordingly. It should be further examined if the effects of velocity and of particle Froude number, which depends upon the flow velocity, add up or jointly contribute to the reduction of 25 %, but this is out of the scope of this paper.

4. Conclusions

The experimental campaign aimed at determining the drag coefficients of wood accumulations at an ogee crested spillway. Such data are lacking in current literature and may help in the management of spillway protection systems or in the prediction of the best conditions to ensure wood passage. Thanks to the possibility of numerical modelling the transport and accumulation of logs near the infrastructures, local dynamics like backwater effect and spillway capacity could be evaluated under different scenarios, thus providing new insights on the management of the basin dynamics.

The drag coefficients were obtained by varying either the submergence of the samples or the distance from the spillway, for cylindrical samples with various size and surface roughness and for wood jam shaped samples. All the samples were meant to be a simplified representation of wood accumulations, to investigate the possibility of employing circular samples instead of more complex wood jam models. In this regard, the experimental campaign shows that the hydrodynamic resistance of rough cylinders is comparable to that of non-porous wood jams only relatively away from the spillway (i.e., for non-dimensional distances larger than 0.2), while at smaller distances the effect of the shape is greater than that of the surface roughness. In addition, if porous wood accumulations are to be examined, cylindrical samples cannot be employed as the solid cross-sectional areas give rise to higher hydrodynamic resistance.

To ensure the reliability of the results, a minimum of 60 repetitions was performed for each test configuration, as determined by the preliminary analysis. The number of repetitions is related to the reliability of the employed instrument and ensures the precision of the current measures. Despite remaining inaccuracies for specific test conditions that involved low velocities and, consequently, low forces on the samples, the general trends of the drag coefficient were derived from the results of the experimental campaign.

The drag coefficient increases with the submergence of the samples, while it decreases with the distance to the spillway crest. The rate of increase of the drag coefficient with submergence appears to be larger than the one measured for logs in open-channel flow, due to the interaction with the spillway that alters the flow distribution. To describe the effect of the distance and the hydrodynamic interaction with the structure, drag coefficient curves as function of the non-dimensional distance from the crest and of the blockage ratio on the spillway were derived. Overall, the distance from the spillway has a stronger influence than the blockage ratio, resulting in a significant reduction of the drag coefficient away from the spillway, even for wood accumulation with large blockage ratio. These findings represent a preliminary hydrodynamic confirmation of the management practices adopted to reduce the backwater effect by keeping the accumulations far from the spillway crest with visors or racks (e.g., Bénet et al., 2021, Boes et al., 2017). Thanks to the lower drag coefficient far from the crest, the drag resistance, and the corresponding backwater effect, are lower, so that the weir rating curve is not affected by the presence of wood.

As shown in the discussion, the scale effects in our experiments are not fully negligible. However, the comparison with a prototype scaled according to the Froude similarity and with a geometrically scaled prototype working at a flow rate corresponding to the design head showed limited variations of the Reynolds and Froude numbers. The application to a prototype scaled according to the Froude similarity is possible, but an increase of the drag coefficient of about 25 % (based upon the difference of velocity) is suggested for safety purposes. To avoid the underestimation of the drag coefficient, our results can be applied to a prototype with a design head flow rate but with particle Froude numbers 0.41–0.43.

Despite the limitations in results applicability, the experimental campaign represents a first step to fill a gap of knowledge on the hydrodynamics of wood accumulations at spillways without a superstructure, required to better understand the dynamic of accumulation and design proper management strategies.

Further investigation is needed to assess the dynamics of wood accumulation at an ogee crested spillway focusing on the hydraulic and geometric conditions that should allow wood passage. An evaluation of the drag forces that arise when changing the flow and the particle Froude number, considering the relation of the design head with a combination of the wood diameter and length, and wood accumulation's shape and orientation, is desirable. This would contribute to identifying a "critical drag coefficient" as a threshold for wood passage over the spillway, related to the flow and log characteristics, rather than only to the design head and log length or diameter, as it is in current literature suggestions.

Furthermore, an in-depth analysis of the dynamics of accumulation at a weir, describing the accumulation processes and not only the blockage probability, and of the characteristics of real wood accumulation, including porosity, would be required. This will help in directing experimental investigation to evaluate also the hydrodynamic coefficients needed for the estimation of additional loads on the structures due to wood accumulation on a spillway, and for the modelling of the related hydraulic effects.

CRediT authorship contribution statement

E. Persi: Conceptualization, Supervision, Validation, Writing – review & editing. **E. Pibia:** Validation, Writing – review & editing. **G. Petaccia:** Conceptualization, Supervision, Validation, Writing – review & editing. **P. Ghilardi:** Supervision, Validation, Writing – review & editing. **S. Sibilla:** Conceptualization, Supervision, Validation, Writing – review & editing.

Declaration of competing interest

The authors declare that they have no known competing financial interests or personal relationships that could have appeared to influence the work reported in this paper.

Data availability

Data will be made available on request.

References

Allen, J., 1947. Scale Models in Hydraulic Engineering. Longmans, Green & Co., London.
Altinisik, A., Kutukceken, E., Umur, H., 2015. Experimental and numerical aerodynamic analysis of a passenger car: Influence of the blockage ratio on drag coefficient. J. Fluid Eng. 137 (8), 081104 https://doi.org/10.1115/1.4030183.
Badanapuri, V.R., 2019. Design principles that are involved in the design of flow over an ogee crest spillway. Int. J. Sci. Res. 8 (8), 245–254. https://doi.org/10.21275/ART2020136.
Bénet, L., De Cesare, G., Pfister, M., 2021. Reservoir level rise under extreme driftwood blockage at ogee crest. J. Hydraul. Eng. 147 (1), 04020086. https://doi.org/10.1061/(asce)hy.1943-7900.0001818.

Bezzola, G.R., Hegg, C., 2007. Ereignisanalyse Hochwasser 2005.[In German.]. Bundesamt für Umwelt and Eidgenös-sische Forschungsanstalt für Wald, Schnee und Landschaft, Bern, Switzerland.
Bocchiola, D., Rulli, M.C., Rosso, R., 2006. Flume experiments on wood entrainment in rivers. Adv. Water Resour. 29 (8), 1182–1195. https://doi.org/10.1016/j.advwatres.2005.09.006.
Bocchiola, D., Rulli, M.C., Rosso, R., 2008. A flume experiment on the formation of wood jams in rivers. Water Resour. Res. 44 (2), 1–17. https://doi.org/10.1029/2006WR005846.
Boes, R., Bühlmann, M., Hochstrasser, H., Kolly, J., Lauber, G., Monney-Ueberl, J., ... Urso, F., 2017. Floating debris at reservoir dam spillways-Report of the Swiss Committee on Dams on the state of floating debris issues at dam spillways. Schweizerisches Talsperrenkomitee-Swiss Committee on Dams, 78.
Boes, R.M., Hager, W.H., 2003. Two-phase flow characteristics of stepped spillways. J. Hydraul. Eng.-ASCE 129 (9), 661–670.
Bradley, J. B., Richards, D. L., Bahner, C.D., 2005. Debris Control Structures-Evaluation and Countermeasures: Hydraulic Engineering Circular 9 (No. FHWA-IF-04-016). United States. Federal Highway Administration. Office of Bridge Technology.
Bruschin, G., Bauer, J., Trucco, S., Trucco, D., 1982. The overtopping of the Palagnedra Dam, pp. 12–19.
Chirici, G., Giannetti, F., Travaglini, D., Nocentini, S., Francini, S., D'Amico, G., Marchetti, M., 2019. Forest damage inventory after the" Vaia" storm in Italy. Forest@ - J. Silvicul. Forest Ecol. 16, 3–9. https://doi.org/10.3832/efor3070-016.
Dankers, R., Feyen, L., 2008. Climate change impact on flood hazard in Europe: An assessment based on high-resolution climate simulations. J. Geophys. Res.-Atmos. 113 (D19) https://doi.org/10.1029/2007JD009719.
Deane, A., Norrey, J., Coulthard, E., McKendry, D.C., Dean, A.P., 2021. Riverine large woody debris introduced for natural flood management leads to rapid improvement in aquatic macroinvertebrate diversity. Ecol. Eng. 163, 106197 https://doi.org/10.1016/j.ecoleng.2021.106197.
Erpicum, S., Tullis, B.P., Lodomez, M., Archambeau, P., Dewals, B.J., Pirotton, M., 2016. Scale effects in physical piano key weirs models. J. Hydraul. Res. 54 (6), 692–698. https://doi.org/10.1080/00221686.2016.1211562.
Everall, N.C., Farmer, A., Heath, A.F., Jacklin, T.E., Wilby, R.L., 2012. Ecological benefits of creating messy rivers. Area 44 (4), 470–478. https://doi.org/10.1111/j.1475-4762.2012.01087.x.
Fais, L.M.C.F. Genovez, A.I.B., 2008. Discharge rating curve and scale effects correction in Morning Glory Spillways. Proceedings of 16th IAHR-APD Congress and 3rd Symposium of IAHR-ISHS, Hohai University, Nanjing, China, 2041-2046.
Flores, L., Larrañaga, A., Díez, J., Elosegi, A., 2011. Experimental wood addition in streams: effects on organic matter storage and breakdown. Freshw. Biol. 56, 2156–2167. https://doi.org/10.1111/j.1365-2427.2011.02643.x.
Furlan, P., Pfister, M., Matos, J., Schleiss, A.J., 2018. Spillway blockage caused by large wood in reservoirs. E3S Web Conf. 40, 1–7. https://doi.org/10.1051/e3sconf/20184002037.
Furlan, P., Pfister, M., Matos, J., Amado, C., Schleiss, A.J., 2019. Experimental repetitions and 633 blockage of large stems at ogee crested spillways with piers. J. Hydraul. Res. 57 (2) https://doi.org/10.1080/00221686.2018.1478897.
Gippel, C.J., O'Neill, I.C., Finlayson, B.L., Schnatz, I., 1996. Hydraulic guidelines for the re-introduction and management of large woody debris in lowland rivers. Regul. Rivers Res. Manag. 12 (2–3), 223–236. https://doi.org/10.1002/(sici)1099-1646(199603)12:2/3<223::aid-rrr391>3.0.co;2-#.
Godtland, K., Tesaker, E., 1994. Clogging of Spillways by Trash. 18th ICOLD Congress, Durban, p. 468.
Grabowski, R.C., Gurnell, A.M., Burgess-Gamble, L., England, J., Holland, D., Klaar, M.J., Wharton, G., 2019. The current state of the use of large wood in river restoration and management. Water Environ. J. 33 (3), 366–377. https://doi.org/10.1111/wej.12465.
Hartlieb, A., 2017. Decisive parameters for backwater effects caused by floating debris jams. Open J. Fluid Dyn. 07 (04), 475–484. https://doi.org/10.4236/ojfd.2017.74032.
Hartung, F., Knauss, J., 1976. Considerations for Spillways Exposed to Dangerous Clogging Conditions. 12th ICOLD Congress, Mexico, p. 447.
Khader, M.A., 1979. Effects of wave drag on submerged bodies. La Houille Blanche 8, 465–470.
Korswagen, P.A., Harish, S., Oetjen, J., Wüthrich, D., 2022. Post-flood field survey of the Ahr Valley (Germany): building damages and hydraulic aspects. Delft Univ. Technol. https://doi.org/10.4233/uuid:3cafd772-facd-4e3a-8b1a-cee978562ff1.
Liro, M., Ruiz-Villanueva, V., Mikuś, P., Wyżga, B., Castellet, E.B., 2020. Changes in the hydrodynamics of a mountain river induced by dam reservoir backwater. Sci. Total Environ. 744, 140555 https://doi.org/10.1016/j.scitotenv.2020.140555.
Manners, R.B., Doyle, M.W., Small, M.J., 2007. Structure and hydraulics of natural woody debris jams. Water Resour. Res. 43 (6), 1–17. https://doi.org/10.1029/2006WR004910.
Manners, R.B., Doyle, M.W., 2008. A mechanistic model of woody debris jam evolution and its application to wood-based restoration and management. River Res. Appl. vol. 24, no. January, 1104–1123. https://doi.org/10.1002/rra.
Müller, S., Follett, E.M., Ouro, P., Wilson, C.A.M.E., 2022. Influence of channel-spanning engineered logjam structures on channel hydrodynamics. Water Resour. Res. 58 https://doi.org/10.1029/2022WR032111 e2022WR032111.
Panici, D., de Almeida, G.A.M., 2018. Formation, growth, and failure of debris jams at bridge piers. Water Resour. Res. 54 (9), 6226–6241. https://doi.org/10.1029/2017WR022177.
Persi, E., Petaccia, G., Fenocchi, A., Manenti, S., Ghilardi, P., Sibilla, S., 2019. Hydrodynamic coefficients of yawed cylinders in open-channel flow. Flow Meas. Instrum. 65, 288–296. https://doi.org/10.1016/j.flowmeasinst.2019.01.006.
Petaccia, G., Fenocchi, A., 2015. Experimental assessment of the stage-discharge relationship of the Heyn siphons of Bric Zerbino dam. Flow Meas. Instrum. 41, 36–40. https://doi.org/10.1016/j.flowmeasinst.2014.10.012.
Pfister, M., Schleiss, A.J., 2013. Estimation of A-type Piano Key weir rating curve. Labyrinth and Piano Key Weirs II–PKW 2013, 139–147.
Ren, H., Xu, Y., Zhang, M., Deng, S., Li, S., Fu, S., Sun, H., 2019. Hydrodynamic forces on a partially submerged cylinder at high Reynolds number in a steady flow. Appl. Ocean Res. 88, 160–169. https://doi.org/10.1016/j.apor.2019.04.025.
Rickli, C., Hess, J., 2009. Aspects de la formation des bois flottants.[In French.] Cours de formation continue KHOS. Protection contre les crues, Fribourg, Switzerland.
Salmasi, F., Abraham, J., 2020. Discharge coefficients for ogee weirs including the effects of a sloping upstream face. Water Supp. 20 (4), 1493–1508. https://doi.org/10.2166/ws.2022.129.
Saneie, M., SheikhKazemi, J., Azhdary Moghaddam, M., 2016. Scale effects on the discharge coefficient of ogee spillway with an arc in plan and converging training walls. Civil Eng. Infrastruct. J. 49 (2), 361–374. https://doi.org/10.7508/ceij.2016.02.012.
Spreitzer, G., Tunnicliffe, J., Friedrich, H., 2021. Effects of large wood (LW) blockage on bedload connectivity in the presence of a hydraulic structure. Ecol. Eng. 161, 106156 https://doi.org/10.1016/j.ecoleng.2021.106156.
Swiss Committee on Dams, 2017. Floating debris at reservoir dam spillways, no. November, pp. 1–78. Available online on August 2023.
U.S. Army Corps of Engineers (1990). Hydraulic Design of Spillways, Engineer Manual No. 1110-2-1603, Washington , D.C., U.S.A.
U.S. Bureau of Reclamation, 1987. Design of Small Dams. US Bureau of Reclamation, Denver, CO, USA, pp. 365–375.
Vischer, D., Hager, W.H., 1998. Dam Hydraulics, Vol. 2. Wiley, Chichester.
Wallerstein, N.P., Alonso, C.V., Bennett, S.J., Thorne, C.R., 2001. Distorted Froude-scaled flume analysis of large woody debris. Earth Surf. Proc. Land. 26 (12), 1265–1283. https://doi.org/10.1002/esp.271.
Wallerstein, N.P., Alonso, C.V., Bennett, S.J., Thorne, C.R., 2002. Surface wave forces acting on submerged logs. J. Hydraul. Eng. 128 (3), 349–353. https://doi.org/10.1061/(ASCE)0733-9429(2002)128:3(349).
Wark, R.J., Ng, K., Hui, S., Swain, R., Graham, R., Pavlov, V., Laugier, F., Machado, B., 2018. Blockage of Reservoir Outlet Structures by Debris Flow. International Commission On Large Dams Commission, 61, avenue Kléber, 75116 Paris. Available online on August 2023.
Wenzel, R., Reinhardt-Imjela, C., Schulte, A., Bölscher, J., 2014. The potential of in-channel large woody debris in transforming discharge hydrographs in headwater areas (Ore Mountains, Southeastern Germany). Ecol. Eng. 71, 1–9. https://doi.org/10.1016/j.ecoleng.2014.07.004.
Wohl, E., et al., 2019. The natural wood regime in Rivers. Bioscience 69 (4), 259–273. https://doi.org/10.1093/biosci/biz013.